This paper is published as part of a PCCP Themed Issue on:
Physical Chemistry of Aerosols

Guest Editors: Ruth Signorell and Allan Bertram (University of British Columbia)

Editorial

Physical Chemistry of Aerosols
Phys. Chem. Chem. Phys., 2009, **DOI:** 10.1039/b916865f

Perspective

Reactions at surfaces in the atmosphere: integration of experiments and theory as necessary (but not necessarily sufficient) for predicting the physical chemistry of aerosols
Barbara J. Finlayson-Pitts, *Phys. Chem. Chem. Phys.*, 2009, **DOI:** 10.1039/b906540g

Papers

Water uptake of clay and desert dust aerosol particles at sub- and supersaturated water vapor conditions
Hanna Herich, Torsten Tritscher, Aldona Wiacek, Martin Gysel, Ernest Weingartner, Ulrike Lohmann, Urs Baltensperger and Daniel J. Cziczo, *Phys. Chem. Chem. Phys.*, 2009, **DOI:** 10.1039/b901585j

Secondary organic aerosol formation from multiphase oxidation of limonene by ozone: mechanistic constraints *via* two-dimensional heteronuclear NMR spectroscopy
Christina S. Maksymiuk, Chakicherla Gayahtri, Roberto R. Gil and Neil M. Donahue, *Phys. Chem. Chem. Phys.*, 2009, **DOI:** 10.1039/b820005j

DRIFTS studies on the photodegradation of tannic acid as a model for HULIS in atmospheric aerosols
Scott Cowen and Hind A. Al-Abadleh, *Phys. Chem. Chem. Phys.*, 2009, **DOI:** 10.1039/b905236d

Infrared spectroscopy of ozone and hydrogen chloride aerosols
Chris Medcraft, Evan G. Robertson, Chris D. Thompson, Sigurd Bauerecker and Don McNaughton, *Phys. Chem. Chem. Phys.*, 2009, **DOI:** 10.1039/b905424n

IR spectroscopy of physical and chemical transformations in cold hydrogen chloride and ammonia aerosols
Evan G. Robertson, Chris Medcraft, Ljiljana Puskar, Rudolf Tuckermann, Chris D. Thompson, Sigurd Bauerecker and Don McNaughton, *Phys. Chem. Chem. Phys.*, 2009, **DOI:** 10.1039/b905425c

Formation of naproxen–polylactic acid nanoparticles from supercritical solutions and their characterization in the aerosol phase
Moritz Gadermann, Simran Kular, Ali H. Al-Marzouqi and Ruth Signorell, *Phys. Chem. Chem. Phys.*, 2009, **DOI:** 10.1039/b901744e

Measurements and simulations of the near-surface composition of evaporating ethanol–water droplets
Christopher J. Homer, Xingmao Jiang, Timothy L. Ward, C. Jeffrey Brinker and Jonathan P. Reid, *Phys. Chem. Chem. Phys.*, 2009, **DOI:** 10.1039/b904070f

Effects of dicarboxylic acid coating on the optical properties of soot
Huaxin Xue, Alexei F. Khalizov, Lin Wang, Jun Zheng and Renyi Zhang, *Phys. Chem. Chem. Phys.*, 2009, **DOI:** 10.1039/b904129j

Spectroscopic evidence for cyclical aggregation and coalescence of molecular aerosol particles
J. P. Devlin, C. A. Yinnon and V. Buch, *Phys. Chem. Chem. Phys.*, 2009, **DOI:** 10.1039/b905018n

Photoenhanced ozone loss on solid pyrene films
Sarah A. Styler, Marcello Brigante, Barbara D'Anna, Christian George and D. J. Donaldson, *Phys. Chem. Chem. Phys.*, 2009, **DOI:** 10.1039/b904180j

Quantifying the reactive uptake of OH by organic aerosols in a continuous flow stirred tank reactor
Dung L. Che, Jared D. Smith, Stephen R. Leone, Musahid Ahmed and Kevin R. Wilson, *Phys. Chem. Chem. Phys.*, 2009, **DOI:** 10.1039/b904418c

Laboratory study of the interaction of HO_2 radicals with the NaCl, NaBr, $MgCl_2 \cdot 6H_2O$ and sea salt surfaces
Ekaterina Loukhovitskaya, Yuri Bedjanian, Igor Morozov and Georges Le Bras, *Phys. Chem. Chem. Phys.*, 2009, **DOI:** 10.1039/b906300e

Kinetics of the heterogeneous reaction of nitric acid with mineral dust particles: an aerosol flowtube study
A. Vlasenko, T. Huthwelker, H. W. Gäggeler and M. Ammann, *Phys. Chem. Chem. Phys.*, 2009, **DOI:** 10.1039/b904290n

Timescale for hygroscopic conversion of calcite mineral particles through heterogeneous reaction with nitric acid
Ryan C. Sullivan, Meagan J. K. Moore, Markus D. Petters, Sonia M. Kreidenweis, Greg C. Roberts and Kimberly A. Prather, *Phys. Chem. Chem. Phys.*, 2009, **DOI:** 10.1039/b904217b

Mid-infrared complex refractive indices for oleic acid and optical properties of model oleic acid/water aerosols
Shannon M. McGinty, Marta K. Kapala and Richard F. Niedziela, *Phys. Chem. Chem. Phys.*, 2009, **DOI:** 10.1039/b905371a

A study of oleic acid and 2,4-DHB acid aerosols using an IR-VUV-ITMS: insights into the strengths and weaknesses of the technique
Sarah J. Hanna, Pedro Campuzano-Jost, Emily A. Simpson, Itamar Burak, Michael W. Blades, John W. Hepburn and Allan K. Bertram, *Phys. Chem. Chem. Phys.*, 2009, **DOI:** 10.1039/b904748d

Deliquescence behaviour and crystallisation of ternary ammonium sulfate/dicarboxylic acid/water aerosols
L. Treuel, S. Pederzani and R. Zellner, *Phys. Chem. Chem. Phys.*, 2009, **DOI:** 10.1039/b905007h

Laboratory chamber studies on the formation of organosulfates from reactive uptake of monoterpene oxides
Yoshiteru Iinuma, Olaf Böge, Ariane Kahnt and Hartmut Herrmann, *Phys. Chem. Chem. Phys.*, 2009, **DOI:** 10.1039/b904025k

Measurement of fragmentation and functionalization pathways in the heterogeneous oxidation of oxidized organic aerosol
Jesse H. Kroll, Jared D. Smith, Dung L. Che, Sean H. Kessler, Douglas R. Worsnop and Kevin R. Wilson, *Phys. Chem. Chem. Phys.*, 2009, **DOI:** 10.1039/b905289e

Using optical landscapes to control, direct and isolate aerosol particles
Jon B. Wills, Jason R. Butler, John Palmer and Jonathan P. Reid, *Phys. Chem. Chem. Phys.*, 2009, **DOI:** 10.1039/b908270k

Reactivity of oleic acid in organic particles: changes in oxidant uptake and reaction stoichiometry with particle oxidation
Amy M. Sage, Emily A. Weitkamp, Allen L. Robinson and Neil M. Donahue, *Phys. Chem. Chem. Phys.*, 2009, **DOI:** 10.1039/b904285g

Surface tension of mixed inorganic and dicarboxylic acid aqueous solutions at 298.15 K and their importance for cloud activation predictions
Alastair Murray Booth, David Owen Topping, Gordon McFiggans and Carl John Percival, *Phys. Chem. Chem. Phys.*, 2009, **DOI:** 10.1039/b906849j

Kinetics of the heterogeneous conversion of 1,4-hydroxycarbonyls to cyclic hemiacetals and dihydrofurans on organic aerosol particles
Yong Bin Lim and Paul J. Ziemann, *Phys. Chem. Chem. Phys.*, 2009, **DOI:** 10.1039/b904333k

Time-resolved molecular characterization of limonene/ozone aerosol using high-resolution electrospray ionization mass spectrometry
Adam P. Bateman, Sergey A. Nizkorodov, Julia Laskin and Alexander Laskin, *Phys. Chem. Chem. Phys.*, 2009, **DOI:** 10.1039/b905288g

Cloud condensation nuclei and ice nucleation activity of hydrophobic and hydrophilic soot particles
Kirsten A. Koehler, Paul J. DeMott, Sonia M. Kreidenweis, Olga B. Popovicheva, Markus D. Petters, Christian M. Carrico, Elena D. Kireeva, Tatiana D. Khokhlova and Natalia K. Shonija, *Phys. Chem. Chem. Phys.*, 2009, **DOI:** 10.1039/b905334b

Effective broadband refractive index retrieval by a white light optical particle counter
J. Michel Flores, Miri Trainic, Stephan Borrmann and Yinon Rudich, *Phys. Chem. Chem. Phys.*, 2009, **DOI:** 10.1039/b905292e

Influence of gas-to-particle partitioning on the hygroscopic and droplet activation behaviour of α-pinene secondary organic aerosol
Zsófia Jurányi, Martin Gysel, Jonathan Duplissy, Ernest Weingartner, Torsten Tritscher, Josef Dommen, Silvia Henning, Markus Ziese, Alexej Kiselev, Frank Stratmann, Ingrid George and Urs Baltensperger, *Phys. Chem. Chem. Phys.*, 2009, **DOI:** 10.1039/b904162a

Reactive uptake studies of NO_3 and N_2O_5 on alkenoic acid, alkanoate, and polyalcohol substrates to probe nighttime aerosol chemistry
Simone Gross, Richard Iannone, Song Xiao and Allan K. Bertram, *Phys. Chem. Chem. Phys.*, 2009, **DOI:** 10.1039/b904741g

Organic nitrate formation in the radical-initiated oxidation of model aerosol particles in the presence of NO_x
Lindsay H. Renbaum and Geoffrey D. Smith, *Phys. Chem. Chem. Phys.*, 2009, **DOI:** 10.1039/b909239k

Dynamics and mass accommodation of HCl molecules on sulfuric acid–water surfaces
P. Behr, U. Scharfenort, K. Ataya and R. Zellner, *Phys. Chem. Chem. Phys.*, 2009, **DOI:** 10.1039/b904629a

Structural stability of electrosprayed proteins: temperature and hydration effects
Erik G. Marklund, Daniel S. D. Larsson, David van der Spoel, Alexandra Patriksson and Carl Caleman, *Phys. Chem. Chem. Phys.*, 2009, **DOI:** 10.1039/b903846a

Tandem ion mobility-mass spectrometry (IMS-MS) study of ion evaporation from ionic liquid-acetonitrile nanodrops
Christopher J. Hogan Jr and Juan Fernández de la Mora, *Phys. Chem. Chem. Phys.*, 2009, **DOI:** 10.1039/b904022f

Homogeneous ice freezing temperatures and ice nucleation rates of aqueous ammonium sulfate and aqueous levoglucosan particles for relevant atmospheric conditions
Daniel Alexander Knopf and Miguel David Lopez, *Phys. Chem. Chem. Phys.*, 2009, **DOI:** 10.1039/b903750k

Homogeneous ice freezing temperatures and ice nucleation rates of aqueous ammonium sulfate and aqueous levoglucosan particles for relevant atmospheric conditions

Daniel Alexander Knopf*[a] and Miguel David Lopez[b]

Received 23rd February 2009, Accepted 10th August 2009
First published as an Advance Article on the web 14th August 2009
DOI: 10.1039/b903750k

Homogeneous ice nucleation from micrometre-sized aqueous $(NH_4)_2SO_4$ and aqueous levoglucosan particles is studied employing the optical microscope technique. A new experimental method is introduced that allows us to control the initial water activity of the aqueous droplets. Homogeneous ice freezing temperatures and ice melting temperatures of these aqueous solution droplets, 10 to 80 μm in diameter, are determined. Homogeneous ice nucleation from aqueous $(NH_4)_2SO_4$ particles 5–39 wt% in concentration and aqueous levoglucosan particles with initial water activities of 0.85–0.99 yield upper limits of the homogeneous ice nucleation rate coefficients of up to 1×10^{10} cm^{-3} s^{-1}. The experimentally derived homogeneous ice freezing temperatures and upper limits of the homogeneous ice nucleation rate coefficients are compared with corresponding predictions of the water-activity-based ice nucleation theory [T. Koop, B. P. Luo, A. Tsias and T. Peter, *Nature*, 2000, **406**, 611]. It is found that the water-activity-based ice nucleation theory can capture the experimentally derived ice freezing temperatures and homogeneous ice nucleation rate coefficients of the aqueous $(NH_4)_2SO_4$ and aqueous levoglucosan particles. However, the level of agreement between experimentally derived and predicted values, in particular for homogeneous ice nucleation rate coefficients, crucially depends on the extrapolation method to obtain water activities at corresponding freezing temperatures. It is suggested that the combination of experimentally derived ice freezing temperatures and homogeneous ice nucleation rate coefficients can serve as a better validation of the water-activity-based ice nucleation theory than when compared to the observation of homogeneous ice freezing temperatures alone. The atmospheric implications with regard to the application of the water-activity-based ice nucleation theory and derivation of maximum ice particle production rates are briefly discussed.

1. Introduction

Atmospheric aerosol particles can affect the global radiation budget, and thus climate, in the following ways.[1] The particles can scatter and absorb solar and terrestrial radiation. Aerosol particles can modify the radiative properties of clouds by serving as cloud condensation nuclei and ice nuclei (IN).[2–10] The importance of ice particles in the atmosphere has been well recognized but the impact of cirrus clouds on the global radiative budget is still not well established.[1] In addition to changes in cloud radiative properties, the formation of ice in the upper troposphere and lower stratosphere (UT/LS) can lead to the dehydration of the UT/LS region by sedimentation of ice particles.[11,12] This process affects the water vapor distribution and, hence, also results in changes of the radiation budget.[13,14] Ice particles at the tropopause will also control the water transport into the lower stratosphere[15–18] with subsequent consequences for the stratospheric chemical composition. In addition, cirrus ice clouds can serve as heterogeneous sites for reactions of nitrogen and halogen species resulting in a destruction of ozone[19] and as sink for the uptake of HNO_3 (*e.g.* Krämer *et al.*[20]).

Atmospheric ice particles can form by homogeneous and heterogeneous nucleation.[9,21] Homogeneous ice nucleation describes the formation of ice from a supercooled purely liquid particle. Heterogeneous ice nucleation can occur by various modes such as deposition nucleation, immersion freezing, or contact freezing.[9,21] Homogeneous ice nucleation has been observed to occur in the atmosphere at high supersaturations with respect to ice.[22–25] In addition, there is evidence for inhibition of ice nucleation and growth in the UT, which might be connected to the presence of organics in aerosols.[26–28] This study focuses on the homogeneous ice nucleation from aqueous ammonium sulfate $[(NH_4)_2SO_4]$ particles which represent a typical background aerosol in the free troposphere[29,30] and aqueous levoglucosan (1,6-anhydro-β-D-glucopyranose, $C_6H_{10}O_5$) particles representing a major organic compound in biomass burning aerosol (BBA) particles.[31,32]

Biomass burning is a major source of gases and particles in the atmosphere with a source strength of similar magnitude to fossil fuel burning.[33–39] Recent findings have demonstrated that biomass burning plumes can affect the atmosphere on a

[a] *Institute for Terrestrial and Planetary Atmospheres/School of Marine and Atmospheric Sciences, Stony Brook University, Nicolls Road, Stony Brook, NY 11794, USA. E-mail: Daniel.Knopf@stonybrook.edu*
[b] *Department of Electrical and Computer Engineering, Stony Brook University, Nicolls Road, Stony Brook, NY 11794, USA*

local to global scale[40–47] thereby reaching the UT and penetrating the LS where temperatures favor ice formation.[42,43,48–50] A large fraction of BBA particles is comprised of complex mixtures of organic and inorganic material.[31,32,51–55] Levoglucosan represents a major water soluble organic compound of BBA particles which can account for up to 60% of the particle mass.[32,55]

Koop *et al.*[56] derived a homogeneous ice nucleation theory for which freezing of ice from supercooled aqueous solutions depends only on particle water activity, a_w, independently of the nature of the solute, also termed water-activity-based ice nucleation theory.[57] For the remainder of the manuscript this theory is abbreviated as KO00. KO00 can be applied to predict homogeneous ice nucleation temperatures and homogeneous ice nucleation rate coefficients from aqueous particles. Its predictive capability strongly depends on a_w in the temperature regime where aqueous particles are supersaturated with respect to ice. Data on a_w for supercooled aqueous solutions are scarce and often have to be determined indirectly. One approach to predict a_w for supercooled aqueous solutions is the application of Pitzer ion-interaction models.[58] The aerosol inorganics model (AIM)[59–62] constitutes among others[63] a Pitzer ion-interaction model which allows us to calculate a_w for supercooled aqueous solutions. AIM can be employed to calculate a_w for supercooled aqueous $(NH_4)_2SO_4$ solutions.[59–62] However, due to the limited amount of thermodynamic data of supercooled aqueous levoglucosan solutions no thermodynamic model is yet available to predict corresponding a_w values at temperatures typical for the UT/LS region.

A few previous studies on homogeneous ice freezing of aqueous organic solution droplets have shown that good agreement between observed ice freezing temperatures and ice freezing temperatures predicted by KO00 can be achieved if changes in a_w with temperature were taken into account.[57,64,65] Here in this study, the validation of KO00 is extended by comparing experimentally derived ice freezing temperatures and upper limits of the homogeneous ice nucleation rate coefficients, J^{up}_{hom}, with corresponding theoretical predictions. Freezing temperatures and corresponding upper limits of the homogeneous ice nucleation rate coefficients for micrometer-sized aqueous $(NH_4)_2SO_4$ and aqueous levoglucosan particles are determined using the optical microscopy approach.[63,66–70] The experiments presented here involve a novel particle generation method which allows us to prepare the aqueous particles as a function of relative humidity (RH) and, hence, particles with known water activities at the preparation temperature. This approach is used to verify the sensitivity of melting and freezing temperatures and the upper limits of the homogeneous ice nucleation rate coefficients on a_w when applying the water-activity-based ice nucleation theory.

2. Experimental

2.1 Apparatus

The experimental setup to study homogeneous ice formation from micrometre-sized aqueous particles is based on previous apparatus[63,66,67,71] and is shown in Fig. 1. A cryo-cooling stage (Linkam BCS196) attached to an optical microscope (OM) operated in transmitted light mode allows the controlled cooling and heating of particles in the temperature range of 170–280 K. A digital camera operated by an imaging software records the freezing, melting, and particle size on a hard drive. The aerosol cell is top-loaded into the cryo-cooling stage which is purged with N_2(g) to avoid condensation of water vapor or ice in the sampling area.

The dimensions of the aerosol cell are chosen in such a way that for typically observed number and sizes of aerosol particles the amount of water vapor within the closed aerosol cell is small compared to the amount of liquid phase water.[63,66,67] For this reason, the composition of the particles remains constant during the freezing experiments since condensation of the remaining water vapor is negligible compared to the condensed phase water. Typical dimensions of the aerosol cell are 1.5 mm in diameter and 0.1–0.2 mm in height. The particle sizes range from 10 to 80 μm in diameter. Up to 100 particles are deposited within the sample area. The hydrophobically[63,67,72] coated glass base plate and cover slide are up to 18 mm in diameter and 0.15 mm thick. Aluminium foil serves as a spacer between the glass plates which were sealed with high vacuum grease.[66] The quality of the hydrophobic monolayer coating by silanization is verified by contact

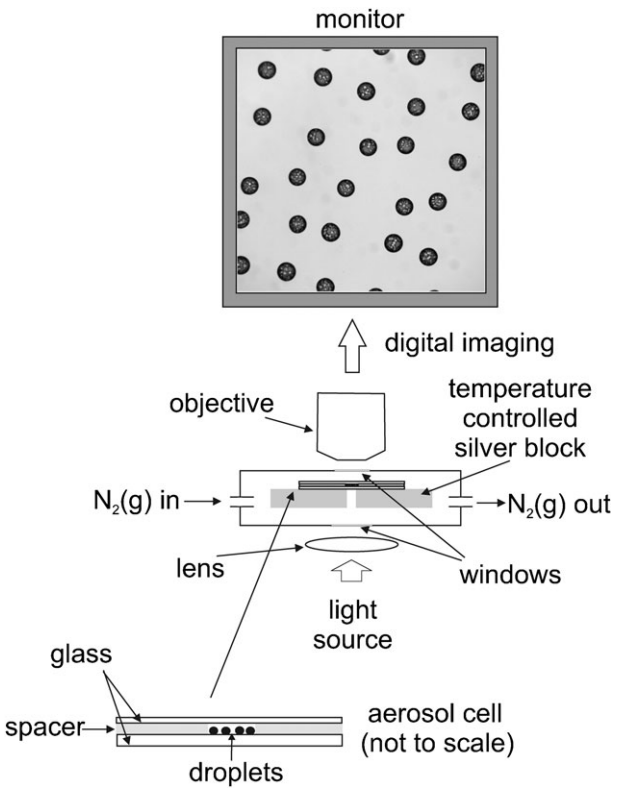

Fig. 1 A sketch of the experimental setup to study homogeneous ice nucleation is shown. It consists of a cryo-cooling stage attached to an optical microscope. An enlarged view of the closed aerosol cell is given which is placed within the cryo-cooling stage. The particle image shows melting of frozen $(NH_4)_2SO_4$–H_2O particles. For more details see text. This sketch is not to scale.

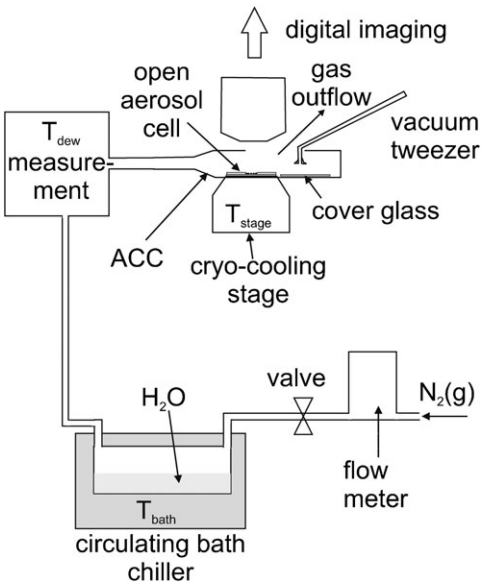

Fig. 2 A sketch of the particle preparation setup is shown. The aerosol conditioning cell (ACC) is placed on a homemade cryo-cooling stage which is attached to a homemade reflected light microscope. A gas flow system provides a humidified N_2(g) flow to the ACC. For more details see text. This sketch is not to scale.

angle measurements applying water droplets and by comparison of measured homogeneous ice freezing temperatures of pure water with literature values.[9]

The particle preparation setup is shown in Fig. 2 which allows the exposure of the aerosol particles to controlled water partial pressures. It consists of a home made optical microscope operated in reflected light mode coupled to a home made cryo-cooling stage which is equipped with an aerosol conditioning cell (ACC). This microscope is equipped with a digital camera and imaging software to monitor and record *in situ* changes in particle phase and size. A controlled humidified gas flow of N_2 larger than 1.6 SLPM (standard litre per minute) is provided to the ACC. This is achieved by passing N_2(g) through a hydrocarbon gas trap and subsequent cold trap filled with molecular sieve before entering a temperature controlled denuder, half filled with water, submersed in a circulating bath chiller. The dew point, T_{dew}, of the humidified gas flow is determined using a chilled mirror hygrometer (GE Sensing). The uncertainty in T_{dew} is smaller than 0.15 K. Its absolute accuracy was verified using an independent chilled mirror hygrometer and a N_2 gas flow with known saturation vapor pressure. The ACC is made out of glass and is entirely hydrophobically coated[63,67,72] to avoid condensation of water vapor which could lead to inhomogeneities of the water partial pressure inside the ACC. The dimensions of the ACC are minimized to ensure spatially homogeneous water partial pressures. The ACC is about 18.5 mm wide, 40 mm long, less than 10 mm in height. The cryo-cooling stage fits snugly inside the bottom of the ACC. At the top of the ACC there is a slit about 25 mm long and about 2 mm wide which allows the cover slide to be lifted up by a vacuum tweezer to close the aerosol cell. The slit also serves as the outlet of the humidified gas.

2.2 Particle generation

The aerosol particles are generated using the following two methods. Aqueous $(NH_4)_2SO_4$ and levoglucosan solutions, about 5 wt% in concentration, are prepared and then atomized using a quartz glass atomizer.[66] Downstream of the atomizer the particles impact the aerosol cell base plate. This results in a polydisperse particle size distribution on the glass plate. A monodisperse particle distribution is generated using a piezo-electric driven single droplet dispenser applied with the same solutions. Most of the sample preparation was performed in a clean bench to avoid contamination of the sample with ambient particles such as dust which could affect homogeneous freezing temperatures by triggering heterogeneous ice nucleation. In addition, exposure to ambient air was kept minimal before placing the sample into the ACC.

The RH to which the particles are exposed is determined from the continuously monitored T_{dew} value of the humidified gas flow and the temperature of the cryo-cooling stage, T_{stage}. From T_{dew} the corresponding water vapor pressure, which represents the water partial pressure inside the ACC, $p^{ACC}_{H_2O}$, can be derived[73]. T_{stage} defines the RH of the humidified gas flow and thus the water activity, a_w, of the solution droplets in equilibrium with the gas.[56] The RH experienced by the particles inside the ACC is obtained from the ratio of $p^{ACC}_{H_2O}$ and the water vapor pressure of pure liquid water, $p^0_{H_2O}$,[73] as:

$$\mathrm{RH} = \frac{p^{\mathrm{ACC}}_{\mathrm{H_2O}}(T_{\mathrm{dew}})}{p^0_{\mathrm{H_2O}}(T_{\mathrm{stage}})} \equiv a_{\mathrm{w}}. \qquad (1)$$

2.3 Calibration

The cryo-cooling stage to measure homogeneous freezing temperatures was calibrated similarly to previously employed nucleation apparatus.[63,66,67] The temperature was calibrated by measuring the melting points[74] multiple times employing at least three independent samples of heptane (182.60 K), octane (216.33 K), decane (243.55 K), dodecane (263.58 K) and ice (273.15 K). The measurements confirmed that the temperature sensor of the cryo-cooling stage was linear for the temperature range of 170–280 K to within less than 0.1 K. The observed freezing temperatures did not show a significant dependency on the cooling rate for cooling rates between 5–50 K min^{-1}.[66] A cooling rate of 10 K min^{-1} was chosen for our ice nucleation experiments to minimize mass transport of water from liquid droplets to frozen particles and temperature offset between the cryo-cooling stage and the droplets.[66,71]

The ACC is calibrated with respect to RH by first determining the melting point of ice particles and subsequently measuring deliquescence relative humidities (DRHs) of various inorganic salts. Ice particles were generated by cooling water droplets 20–80 μm in diameter to about 230 K to induce freezing. These water droplets were formed by condensation of water vapor in the supersaturated environment of the ACC. The ice melting point, T^{melt}_{ice} was determined using a heating ramp of 0.1 K min^{-1}. This procedure was repeated for at least 3 times using at least 3 different individual samples of water droplets. The deviation of T_{stage} from T^{melt}_{ice} was less than 0.05 K. DRHs

Table 1 Deliquescence relative humidities (DRHs) of K_2CO_3, K_2SO_4, LiCl and $(NH_4)_2SO_4$ observed at 306 K, 293 K, 300 K, and 295 K, respectively

Compound	DRH^{obs} (%)	DRH^{lit} (%)
K_2CO_3	43.4 ± 0.3	43.2 ± 0.5[a]
K_2SO_4	97.5 ± 0.4	97.6 ± 0.3[a]
LiCl	11.0 ± 0.1	11.3 ± 0.3[a]
$(NH_4)_2SO_4$	80.1 ± 0.7	80.0 ± 1.5[b]

[a] Greenspan.[98] [b] Tang and Munkelwitz,[99] Xu *et al.*,[100] Cziczo and Abbatt[79] and Onasch *et al.*[101]

of various inorganic salts were determined applying the calibrated T_{stage} and T_{dew} (see Table 1). Monodisperse and polydisperse aerosol particles of the respective inorganic salts in similar size to particles employed in the experiments were applied for these DRH measurements. The RH was continuously increased by decreasing T_{stage} by maximum 0.1 K min^{-1} which results in a change of about 0.6% RH min^{-1}. Each DRH value was obtained from at least 8 measurements using at least 2 independent samples containing up to 50 particles. Table 1 shows the very good agreement between observed and expected DRH values for various inorganic salts covering a wide range of RH values. Careful observation during the deliquescence process ensured that all particles took up water vapor simultaneously. This indicates little or no temperature gradient across the aerosol cell. These results also indicate no significant entrainment of laboratory humidity into the ACC under typical experimental conditions.

2.4 Experimental procedure

Experiments on homogeneous ice nucleation from aqueous $(NH_4)_2SO_4$ particles were conducted employing two methods. The first approach follows previous OM studies.[66,67,69,71] The homogeneous ice freezing temperatures and the corresponding melting temperatures were determined. Subsequently, the individual particle composition was derived from the melting temperatures.[59–62] The second method utilized the ACC allowing the exposure of the aqueous particles to fixed RHs. Subsequently, the corresponding ice freezing and melting temperatures were determined. The ice freezing experiments involving aqueous levoglucosan particles were solely conducted employing the ACC.

The aerosol particles are placed in the ACC and T_{stage} is continuously decreased to achieve RHs above the DRH of the particles to ensure complete deliquescence of the particles and/or continuous particle growth. Then T_{stage} is adjusted to yield the desired RH according to eqn (1). The time for aqueous particles to achieve equilibrium with a given partial pressure depends on composition, temperature, and size of the particles.[9,75] Continuously recorded OM images during RH exposure were used to validate that no further changes in particle size occurred. When the droplets reach equilibrium the aerosol cell is closed, thereby fixing the particle composition and thus a_w. After closure of the aerosol cell an additional image of the particles is taken to ensure that the closing of the cell did not alter the droplet sizes and to confirm the leak tightness of the aerosol cell. Subsequently, the aerosol sample is transferred to the ice nucleation OM setup and the particle size is verified another time before starting the homogeneous ice nucleation experiment. The particles were cooled at a rate of 10 K min^{-1} until freezing of all the particles was observed. The melting point was determined by heating the particles at rates between 0.1 and 1 K min^{-1}. The experiments were monitored by recording an image every 0.1–0.5 K. Thus, the temperature uncertainty is defined by the image recording frequency. Post analysis of the recorded images yields freezing and melting temperatures and diameters of the individual particles. Particle volume was calculated from the spherical equivalent diameter which was derived from the digitally measured particle diameter corrected for the non-sphericity of the deposited particles.[66,67]

2.5 Chemicals

N_2 (99.999%) was purchased from Praxair. All chemicals were purchased from VWR. Listed below are the chemicals and the corresponding purities used in our studies: LiCl (99.995%), $(NH_4)_2SO_4$ (99.95%), K_2CO_3 (99.997%), K_2SO_4 (99.99%), levoglucosan (99%), decane (99%), dodecane (99 + %), octane (98 + %), heptane (99 + %). Millipore water (resistivity $\geq$ 18.2 MΩ cm) was used for preparation of aqueous solutions.

3. Results and discussion

3.1 Aqueous ammonium sulfate particles

Fig. 3 shows the calibrated ice freezing and melting temperatures for over 1500 individually analyzed aqueous $(NH_4)_2SO_4$ droplets. Open squares represent data obtained employing the melting point method[71] and diamonds are obtained by using the ACC. The melting temperature curve as a function of particle composition is derived using AIM.[59–62] The uncertainty in composition of data obtained using the ACC is derived from the uncertainty in RH. A range of freezing temperatures for one specific particle composition is commonly observed due to the stochastic nature of the homogeneous ice nucleation process.[9,76] Furthermore, the polydispersity of the particles employed in this study leads to different homogeneous freezing temperatures; with larger particles having a greater probability of freezing at higher temperatures compared to smaller particles.[9] Also, the observed range of freezing temperatures may be in part due to heterogeneous nucleation of ice from the investigated droplets.[66,71]

Fig. 4 shows the median freezing temperatures with corresponding 20th and 80th percentiles calculated from our freezing data of aqueous $(NH_4)_2SO_4$ particles, shown in Fig. 3, binned in 1 wt% intervals in comparison with literature data.[71,72,77–83] The data of this work falls nicely within the range of previous laboratory studies employing various techniques such as OM,[71,72] differential scanning calorimetry (DSC),[71] falling droplet apparatus,[77] X-ray diffraction,[83] Fourier transform infra-red spectroscopy (FTIR) aerosol flow tubes[78,79,81,84] and the continuous flow diffusion chamber.[82] However, some of the homogeneous ice nucleation experiments employing FTIR aerosol flow tubes[78,81] deviate significantly from the

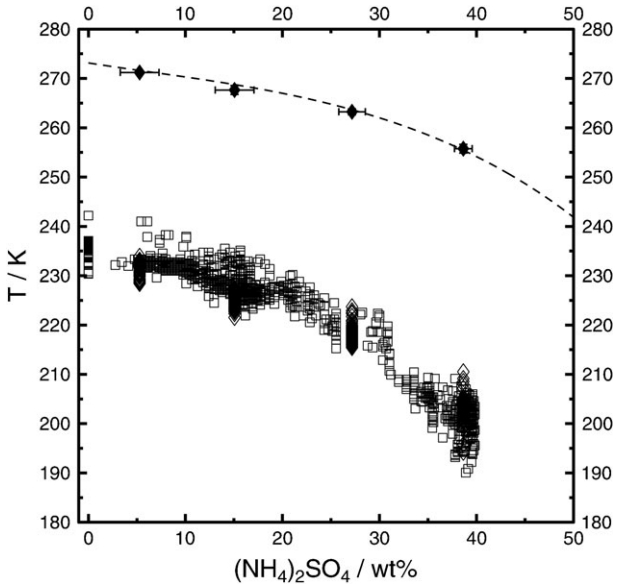

Fig. 3 Ice freezing and corresponding ice melting temperatures of aqueous $(NH_4)_2SO_4$ particles are given as a function of concentration as open and closed symbols, respectively. Open squares indicate ice nucleation experiments in which particle composition was determined by the corresponding ice melting temperatures. Diamonds indicate ice nucleation experiments using ACC. The dashed line indicates the thermodynamically expected ice melting temperatures for aqueous $(NH_4)_2SO_4$ solutions.[59–62]

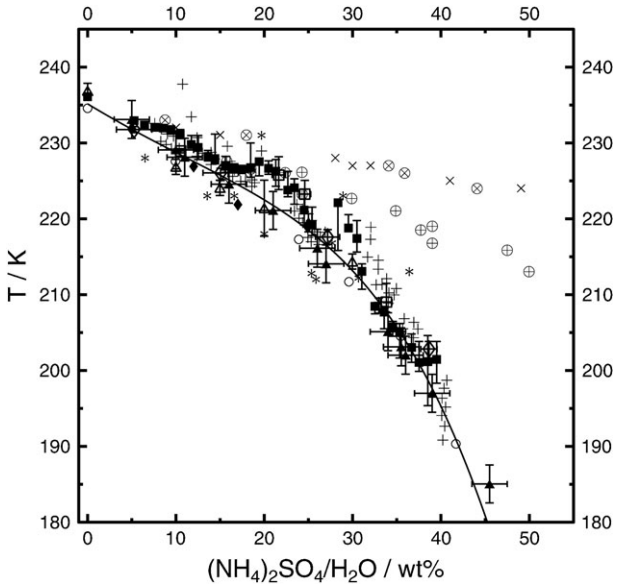

Fig. 4 Summary of ice nucleation data for aqueous $(NH_4)_2SO_4$ particles. Solid squares represent median freezing temperatures with corresponding 20th and 80th percentiles calculated from the freezing temperatures shown in Fig. 3 and binned in 1 wt% intervals. Open diamonds represent median freezing temperatures obtained in this study using ACC with corresponding 20th and 80th percentiles. Open squares and pluses represent data from OM measurements.[71,72] Open circles represent data derived from DSC measurements.[71] Open triangles represent data obtained by falling droplet apparatus.[77] Solid diamonds, crosses, circled pluses, and circled crosses represent nucleation data derived form aerosol flow tube studies.[78,79,81,84] Asterisks represent data obtained using a continuous flow diffusion chamber.[82] The solid triangle represents ice nucleation data from X-ray diffraction experiments.[83] The solid line indicates the freezing temperature curve for aqueous ammonium sulfate particles as given by Bertram *et al.*[71]

previous data sets and this work. This disagreement is addressed in detail in the literature.[78,81,85] Abbatt *et al.*[85] conclude that in these specific experiments, partly crystallized $(NH_4)_2SO_4$ particles nucleated ice heterogeneously leading to higher freezing temperatures when compared to observed homogeneous ice nucleation temperatures. Fig. 3 and 4 show a very good agreement of the freezing data obtained in this study with literature data of homogeneous ice nucleation from aqueous $(NH_4)_2SO_4$ particles and indicate the successful application of the ACC.

Fig. 5 shows the median freezing temperatures with corresponding 20th and 80th percentiles as shown in Fig. 4 but as a function of a_w. In addition, freezing data by Larson and Swanson[77] are given in Fig. 5. AIM[59–62] is employed for all data to predict a_w^{AIM} at the experimentally derived freezing temperatures. In addition, Fig. 5 presents predicted changes in a_w as a function of temperature for selected aqueous $(NH_4)_2SO_4$ concentrations using AIM.[59–62] For the same aqueous $(NH_4)_2SO_4$ concentrations Fig. 5 also presents lines of constant a_w assuming that $a_w(T_{freeze}) = a_w^{ice}(T_{melt})$. This procedure is suggested by Koop *et al.*[56] to estimate a_w at the freezing point if no low temperature data of a_w are available. However, this assumes that a_w is not a strong function of temperature. $a_w^{ice}(T)$ at the melting point is given by Koop *et al.*[56] as

$$a_w^{ice}(T) = \exp[(210\,368 + 131.438T - 3.32373 \times 10^6 T^{-1} - 41\,729.1 \ln T)/RT], \quad (2)$$

where T is temperature and R is the ideal gas constant.

The homogeneous freezing curve depicted in Fig. 5 can be derived according to Koop *et al.*[56] by

$$a_w^{freeze}(T) = a_w^{ice}(T) + \Delta a_w, \quad (3)$$

where $\Delta a_w = 0.305$.[56] Δa_w is also termed the water activity criterion of the water-activity-based ice nucleation theory.[56] Note that this value of $\Delta a_w = 0.305$ corresponds to a fixed J_{hom} value for particles 1–10 μm in diameter that is probably not representative of the larger particles investigated here (10–80 μm in diameter), but depends both on droplet size and cooling rate. Therefore, the aqueous droplets employed in this study should freeze at slightly higher temperatures resulting in a correspondingly lower $\Delta a_w = 0.295$. This is within the range of our experimental uncertainty of about ±0.01. The chosen uncertainties for the theoretically derived freezing temperatures presented in Fig. 5 are obtained by applying eqn (3) using $\delta(\Delta a_w) = \pm 0.025$. (For the remainder of the manuscript the uncertainty in Δa_w is designated as $\delta(\Delta a_w)$.) Koop[57] showed that all data in Koop *et al.*[56] can be represented within an interval of $\delta(\Delta a_w) = \pm 0.05$ and that at higher temperatures the data fall within a smaller interval of $\delta(\Delta a_w) = \pm 0.025$. Hence, a value of $\delta(\Delta a_w) = \pm 0.025$ may be too optimistic. In addition, it might be a too optimistic value with regard to the lack of direct a_w measurements for

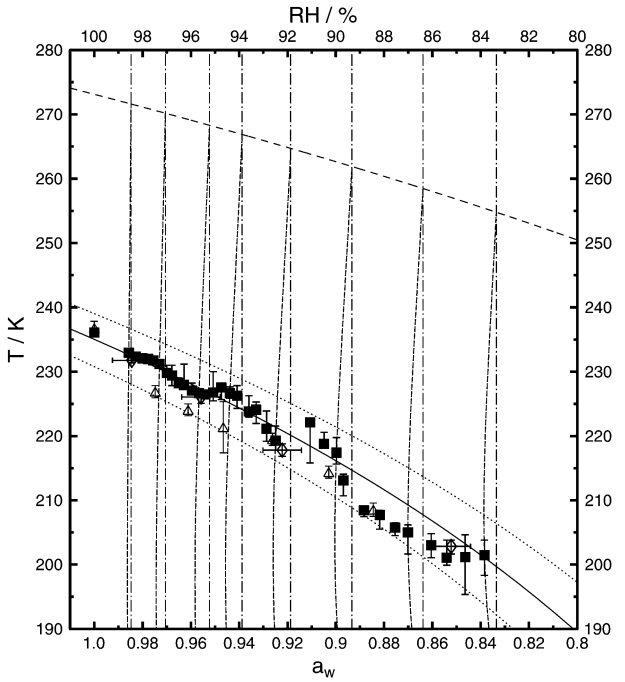

Fig. 5 Solid squares represent median freezing temperatures of aqueous $(NH_4)_2SO_4$ particles with corresponding 20th and 80th percentiles obtained in this study as a function of water activity. Open diamonds represent freezing temperatures with corresponding 20th and 80th percentiles obtained in this study using ACC for particle preparation. Open triangles represent ice nucleation data by Larson and Swanson.[77] The data are plotted as a function of a_w using AIM.[59–62] The wide dashed line and solid line represent the ice melting and homogeneous ice nucleation curve, respectively, given by Koop *et al.*[56] Dotted lines indicate the uncertainty in the homogeneous ice nucleation curve assuming $\delta(\Delta a_w) = \pm 0.025$. Dashed-dotted lines represent constant a_w values determined at the melting temperatures of aqueous $(NH_4)_2SO_4$ particles 5.3, 10.5, 16.6, 20.5, 25.4, 30.5, 35.3, and 39.5 wt% in concentration. Narrow dashed lines represent changes in particle a_w with temperature as predicted by AIM.[59–62]

supercooled aqueous inorganic solutions and potential uncertainties of and disagreements among Pitzer ion-interaction models.[61–63,86]

Fig. 5 shows that the median freezing temperatures of aqueous $(NH_4)_2SO_4$ solution aerosol particles plotted employing $a_w^{AIM}(T_{freeze})$ agree for the most part closely with the theoretically expected freezing temperatures. For $a_w < 0.9$ the experimental data may indicate a trend to lower ice freezing temperatures compared to the theoretical derived ones. However, this depends crucially on the chosen $a_w(T_{freeze})$ values. Fig. 5 indicates significant differences in a_w for the experimentally derived median freezing temperatures when using $a_w^{AIM}(T_{freeze})$ or the assumption $a_w(T_{freeze}) = a_w^{ice}(T_{melt})$. Applying the latter assumption for $a_w < 0.9$, the experimentally derived median freezing points would shift to lower a_w values and result in better agreement with the corresponding predicted ice freezing temperatures.

The open triangles in Fig. 5 represent data of Larson and Swanson which were obtained by the falling droplet apparatus.[77] These data exhibit lower ice freezing temperatures over the presented a_w range compared to the ice freezing temperature curve suggested by Koop *et al.*[56] and most of our data. However, the ice freezing point of pure water determined by Larson and Swanson[77] is in agreement with previous measurements.[9] Overall there is good agreement between experimentally derived and predicted ice freezing temperatures as a function of a_w when experimental uncertainties and uncertainties in the predictions by KO00 are taken into account.

The ice freezing data obtained here are used to derive upper limits of the homogeneous ice nucleation rate coefficients, J_{hom}^{up}, as will be outlined below. These J_{hom}^{up} values also account for possible heterogeneous ice nucleation events which for most experiments on homogeneous ice nucleation from liquid droplets cannot be ruled out. Heterogeneous ice nucleation would lead to apparently higher homogeneous ice nucleation rate coefficients at same temperatures. Therefore, it is advantageous to apply upper limits of the homogeneous ice nucleation rate coefficients for interpretation of the freezing data instead of homogeneous ice nucleation rate coefficients, J_{hom}. For these reasons, measured or modeled homogeneous ice nucleation rate coefficients yielding values lower than J_{hom}^{up} at same temperatures are in agreement with J_{hom}^{up} as will be further outlined below.

The analysis of the experimental data follows a previous method and is described here in short.[66,67,70] J_{hom}^{up} is derived from the experimental data using the following formula:

$$J_{hom}^{up}(T) = \frac{n^*}{\sum_i V_i t_i(T)}, \qquad (4)$$

where n^* is the upper fiducial limit of the actual number of observed ice nucleation events, n.[76] $t_i(T) = \int_T^{T_{freeze}^i} (dT'/dt)_i^{-1}\, dT'$ is the time interval that the ith droplet with volume V_i remained liquid between T and T_{freeze}^i. T_{freeze}^i is the nucleation temperature of the droplet, and $(dT/dt)_i$ is the cooling rate applied in the particular experiment. The integration following eqn (4) is performed in 0.1 K steps from the melting temperature until T_{freeze}^i of the individual droplets of same composition. Within the integration of eqn (4) the difference between the integrative variable T and T_{freeze}^i decreases resulting in smaller t_i values and thus larger J_{hom}^{up} values. The total number of ice nucleation events (n or n^*) and total liquid volume of the droplets are determined for each integration step. With decreasing temperature the total number of ice nucleation events decreases, thus decreasing the total liquid volume, V_i, and resulting in an increase of J_{hom}^{up} according to eqn (4). J_{hom} values are derived from eqn (4) applying n instead of n^*.

The underlying processes of homogeneous ice nucleation from an aqueous solution can be described by a stochastic process.[9,76] Since in experiments the observation time is finite, the stochastic nature of the nucleation process can be exploited to estimate the maximum number of observable nucleation events for a given confidence level.[76] Here we account for these maximum number of nucleation events by employing n^* which is the upper fiducial limit of n determined by Poisson statistics at a confidence level of 0.999.[76] If the experiments were repeated an infinite number of times the observed number of nucleation events will be smaller than n^* in 99.9% of the cases. For example, $n = 4$ observed nucleation events would result,

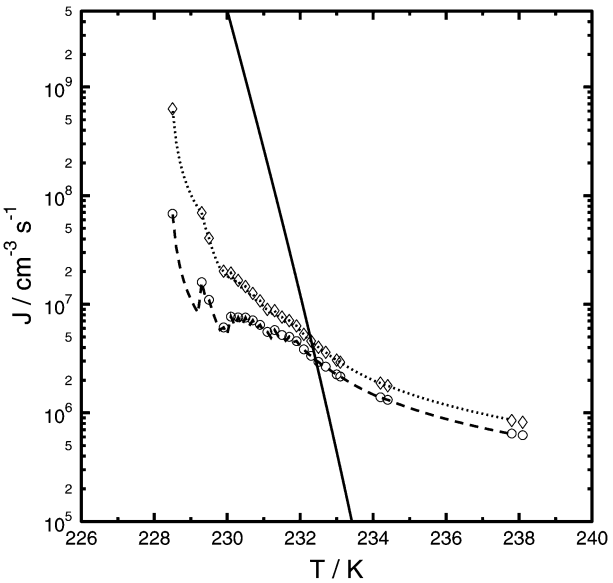

Fig. 6 Experimentally derived J_{hom} and J_{hom}^{up} values for aqueous $(NH_4)_2SO_4$ particles 10 wt% in concentration are shown as open circles and open diamonds, respectively. The dashed and dotted lines represent J_{hom} and J_{hom}^{up} values obtained from integration of eqn (4). The solid line represents the theoretical prediction of J_{hom} by the water-activity-based ice nucleation theory[56] for aqueous $(NH_4)_2SO_4$ particles 10 wt% in concentration.

according to Poisson statistics at a confidence level of 0.999, in $n^* = 15$ nucleation events (see Table 2 in Koop *et al.*[76]). For the same reason, J_{hom}^{up} values can be derived although no ice nucleation events are observed. Application of n^* can significantly change the measured J_{hom} values. For these reasons, eqn (4) yields a conservative (*i.e.* the highest possible) J_{hom} value which is compatible with the experimental data. In other words, only J_{hom} values smaller than J_{hom}^{up} values evaluated at same T agree with each other within the combined error limits.

Fig. 6 shows the experimentally derived J_{hom} and J_{hom}^{up} values for aqueous $(NH_4)_2SO_4$ particles 10 wt% in concentration as open circles and open diamonds, respectively, and the corresponding theoretical prediction of J_{hom} by KO00. The dashed and dotted lines represent J_{hom} and J_{hom}^{up} values obtained from integration of eqn (4) applying n and n^*, respectively. The fluctuations in J_{hom} for $T < 230$ K reflect the competing influence of decreasing liquid particle volume and number of frozen particles on eqn (4). A larger number of observed freezing events would result in a smoother J_{hom} curve at these temperatures. This is evident for the corresponding J_{hom}^{up} values which show much fewer fluctuations since the upper fiducial limit of n is applied in this derivation. The difference between the calculated J_{hom} and J_{hom}^{up} values is maximum at the lowest freezing temperatures due to the sensitivity of eqn (4) to n^*.

The analysis of the freezing data includes possible heterogeneous ice nucleation events. For example, freezing points at about 234 K and 238 K shown in Fig. 6 may be associated with heterogeneous ice nucleation. This effect can lead to erroneous J_{hom} values. Fig. 6 shows for comparison the predicted J_{hom} values applying KO00. The experimentally derived J_{hom} values agree with the predicted J_{hom} values where both data sets intersect. The interpretation of the calculated J_{hom}^{up} values is different. J_{hom}^{up} values are in agreement with the predicted J_{hom} values at the intersection of both data sets. For all higher temperatures J_{hom}^{up} serves as an upper limit of the actual J_{hom} values under the generally valid assumption that J_{hom} increases monotonously with decreasing temperature. For example, from Fig. 6 it can be concluded that the actual J_{hom} values must be smaller than 1×10^6 cm^{-3} s^{-1} at about 236 K. Thus, J_{hom}^{up} allows us to place a limit on the actual J_{hom} values over a wider temperature range compared to the application of the experimentally derived J_{hom} values. Both experimentally derived J_{hom} and J_{hom}^{up} values suggest that predicted J_{hom} values are too high when approaching the lowest observed freezing points. For example, at about 230 K the predicted J_{hom} values are two orders of magnitude higher than the experimentally derived J_{hom}^{up} values.

For the remainder of the manuscript J_{hom}^{up} values should be interpreted as upper limits of the homogeneous ice nucleation rate coefficients and not as homogeneous ice nucleation rate coefficients, J_{hom}.

Theoretically obtained J_{hom} values are derived following the approach by Koop *et al.*[56] J_{hom} is calculated as a function of Δa_w employing

$$\log[J_{hom}(\Delta a_w)] = -906.7 + 8502\Delta a_w - 26\,924(\Delta a_w)^2 + 29\,180(\Delta a_w)^3. \quad (5)$$

For $\Delta a_w = 0.305$, eqn (5) yields $J_{hom} \simeq 5 \times 10^9$ cm^{-3} s^{-1}.[56] As discussed above, application of a different droplet size and/or cooling rate will change the corresponding homogeneous freezing temperature and thus a_w resulting in a different J_{hom} value.[56] The temperature dependency of J_{hom} is derived by using eqn (2) and (3) and the relationship of

$$\Delta a_w(T) = a_w^{freeze}(T) - a_w^{ice}(T). \quad (6)$$

Employing $a_w^{freeze}(T)$ and $a_w^{ice}(T)$ of Koop *et al.*[56] in eqn (6) will result in a constant $\Delta a_w(T)$ value of 0.305 which yields a constant J_{hom} value. Modification of $\Delta a_w(T)$ by changes in $a_w^{freeze}(T)$ due to the application of different estimation methods for a_w will lead to smaller or larger $a_w(T_{freeze})$ values and, thus, smaller or larger $J_{hom}(\Delta a_w)$ values at T_{freeze}, respectively.

Fig. 7a shows the experimentally derived J_{hom}^{up} values for selected aqueous $(NH_4)_2SO_4$ particle compositions ranging from about 5 wt% to 39 wt% in concentration. In the temperature range of about 5 K above the lowest observed freezing temperatures indicated by the solid circles in Fig. 7, J_{hom}^{up} increases by more than two orders of magnitude. J_{hom}^{up} values presented in Fig. 7 are in agreement with the theoretical predictions at the temperature where both data sets intersect and all higher temperatures. The apparent discontinuity of J_{hom}^{up} values for 39 wt% aqueous $(NH_4)_2SO_4$ droplets at about 198 K may be due to a combined effect of small droplet size, uncertainty in droplet composition, heterogeneous ice nucleation, or crystallization of ammonium sulfate.[62] The latter cannot be discriminated from ice nucleation by optical microscopy. Fig. 7a presents theoretically predicted J_{hom} values and

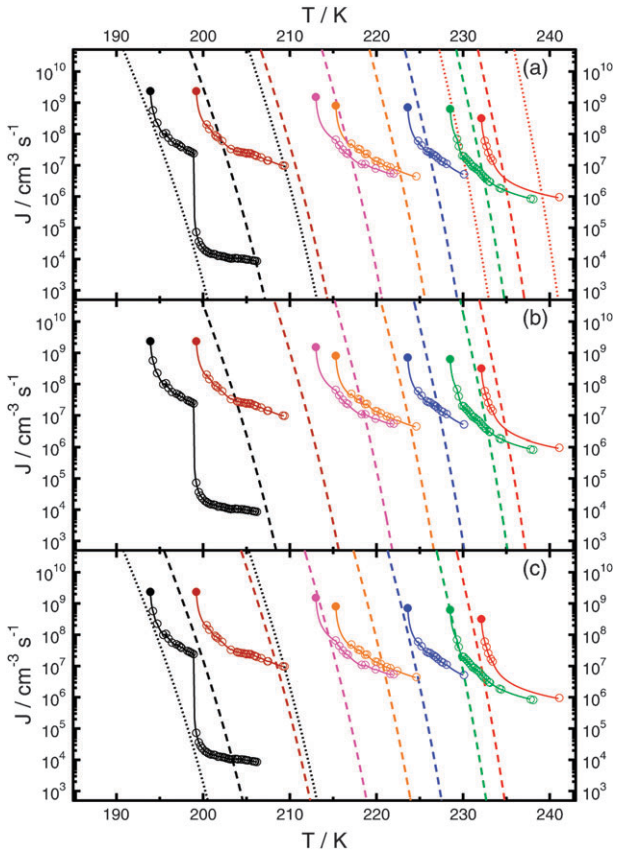

Fig. 7 Circles and dashed lines represent experimentally derived upper limits of the homogeneous ice nucleation rate coefficients and theoretically derived homogeneous ice nucleation rate coefficients,[56] respectively. The solid lines represent corresponding J_{hom}^{up} values obtained from integration of eqn (4). The colors red, green, blue, orange, magenta, brown and black correspond to aqueous $(NH_4)_2SO_4$ particles 5.3, 10.5, 20.5, 25.4, 30.5, 35.3 and 39.5 wt% in concentration, respectively. Solid circles represent the lowest observed freezing points of the respective aqueous $(NH_4)_2SO_4$ particles. Panel (a): dotted lines represent uncertainties in J_{hom} when $\delta(\Delta a_w) = \pm 0.025$ is employed for aqueous $(NH_4)_2SO_4$ particles 5.3 and 39.5 wt% in concentration. Theoretically derived J_{hom} values are calculated applying the water-activity-based ice nucleation theory assuming $\Delta a_w(T) = a_w^{ice}(T_{melt}) - a_w^{ice}(T)$.[56] See text for more details. Panel (b): theoretically derived J_{hom} values are calculated applying the water-activity-based ice nucleation theory assuming $\Delta a_w(T) = a_w^{AIM}(T) - a_w^{ice}(T)$. See text for more details. Panel (c): theoretically derived J_{hom} values are calculated applying the water-activity-based ice nucleation theory assuming $\Delta a_w(T) = a_w^{AIM}(T_{freeze}) - a_w^{ice}(T) - 0.015$. Black dotted lines represent the same uncertainties as shown in panel (a). See text for more details.

corresponding uncertainties assuming a $\delta(\Delta a_w) = \pm 0.025$. These J_{hom} values are calculated employing eqn (5) and

$$\Delta a_w(T) = a_w^{ice}(T_{melt}) - a_w^{ice}(T). \quad (7)$$

This represents the case for which a_w at the freezing point is defined by a_w derived at the melting point of the solution droplet. This approach assumes no significant changes in a_w with decreasing temperature.[56] This case is indicated in Fig. 5 by the vertical lines for $a_w(T) = \text{const}$. The predicted J_{hom} values in Fig. 7a represent changes in J_{hom} when following the line of constant a_w shown in Fig. 5. The temperature dependency of Δa_w is introduced by variation of a_w^{ice} with T according to eqn (2) within eqn (7).

When comparing experimentally derived J_{hom}^{up} values with theoretically derived J_{hom} values, the end points or highest values of the respective J_{hom}^{up} data are applied. Fig. 7a shows that all predicted J_{hom} values are significantly larger than the experimentally derived J_{hom}^{up} values at same temperatures when approaching the lowest freezing temperatures. Deviations between J_{hom} and J_{hom}^{up} values are larger for higher particle solute concentration, *i.e.* lower a_w, when compared to more diluted particles concentrations. However, taking into account an uncertainty of $\delta(\Delta a_w) = \pm 0.025$ these deviations can be explained as indicated by the dotted lines in Fig. 7a. Therefore, the reasons for these deviations may not lie within the water-activity-based ice nucleation theory but may be due to the uncertainty of a_w for supercooled particles. The strong sensitivity of J_{hom} on a_w will be discussed in more detail below.

Fig. 7a indicates that only measuring homogeneous freezing temperatures may not be sufficient to corroborate or refute KO00. The freezing data presented in Fig. 5 as a function of a_w would suggest a much closer agreement between experiment and prediction by KO00 compared to the analysis of J_{hom} presented in Fig. 7a. Fig. 7a shows that homogeneous ice nucleation may occur at temperatures up to 8 K lower than theoretically expected.

Fig. 7b compares experimentally derived J_{hom}^{up} values with J_{hom} values calculated using eqn (5) and

$$\Delta a_w(T) = a_w^{AIM}(T) - a_w^{ice}(T). \quad (8)$$

Eqn (8) indicates that changes in particle a_w with temperature are given by AIM,[59–62] $a_w^{AIM}(T)$. This case is presented as narrow dashed lines in Fig. 5. Fig. 7b shows that the predicted J_{hom} values deviate more from the J_{hom}^{up} values compared to the case presented in Fig. 7a. At fixed temperatures the application of eqn (8) leads to higher J_{hom} values compared to the case when employing eqn (6). This can be also inferred from Fig. 5 which clearly shows $a_w^{AIM}(T) > a_w^{ice}(T)$ implying larger Δa_w values and thus larger J_{hom} values.

A recent study by Larson and Swanson[77] suggests applying $\Delta a_w = 0.32$ instead of 0.305 to derive the curve for homogeneous ice nucleation temperatures for aqueous $(NH_4)_2SO_4$ particles from the melting point curve given by eqn (2). It can be assumed that the uncertainty of the new $\Delta a_w = 0.32$ is similar to the experimental uncertainty.[77] It should also be noted that the translation of the ice freezing curve would lead to disagreement with the measured ice freezing temperature of pure water[77] which is essential for the derivation of KO00.[56,57] A shift of Δa_w by 0.015 moves the homogeneous freezing curve of constant $J_{hom} \simeq 5 \times 10^9$ cm^{-3} s^{-1} to lower temperatures at which previously $J_{hom} \simeq 1 \times 10^{13}$ cm^{-3} s^{-1}. The corresponding Δa_w values with a_w determined at the freezing point[77] employing AIM[59–62] can be expressed as

$$\Delta a_w(T) = a_w^{AIM}(T_{freeze}) - a_w^{ice}(T) - 0.015. \quad (9)$$

Application of eqn (9) and (5) yield the J_{hom} values presented in Fig. 7c. In addition, Fig. 7c shows the uncertainties in J_{hom}

for aqueous $(NH_4)_2SO_4$ particles 39 wt% in concentration, derived for the case shown in Fig. 7a as dotted lines for comparison. Applying $\Delta a_w = 0.32$ results in predicted J_{hom} values which apparently come closer to the experimentally derived freezing data but are still in disagreement. Also, the newly predicted J_{hom} values lie within the uncertainty range given by KO00[56,57] applying $\Delta a_w = 0.305$. From this it can not be deduced if $\Delta a_w = 0.32$ represents a superior water activity criterion, in particular when considering that the newly suggested ice freezing curve would be in disagreement with the freezing of pure water.[9,77] More accurate a_w data for supercooled aqueous $(NH_4)_2SO_4$ particles are needed to resolve this issue.

The results shown in Fig. 7 clearly indicate the sensitivity of KO00 on chosen particle a_w. Applying three different approaches to determine a_w at the ice freezing temperatures of aqueous $(NH_4)_2SO_4$ particles of various concentrations show different levels of agreement between experimentally derived J_{hom}^{up} and predicted J_{hom} values. Fig. 7 indicates that temperature differences of up to 8 K between experimentally derived J_{hom}^{up} and theoretically obtained J_{hom} values can occur. However, when applying different approaches to estimate a_w the experimentally derived ice freezing temperatures appear to be in rather good agreement with the suggested homogeneous ice nucleation curve given by eqn (3), *i.e.* the deviation from a_w^{freeze} is in most part smaller than $\delta(\Delta a_w) = \pm 0.05$.[57] For this reason the experimentally derived J_{hom}^{up} values can serve as a tighter constraint of KO00. The results presented in Fig. 7 indicate that most likely uncertainties in a_w of supercooled aqueous solution droplets are the main reason for disagreement of experimental and theoretical data and not the underlying physical arguments of KO00.[57,87] More accurate $a_w(T)$ values may lead to a shift or even in a change in the curve progression of the homogeneous ice nucleation curve for fixed homogeneous ice nucleation rate coefficients. Such changes would be in accordance with the water-activity-based ice nucleation theory since the driving parameter of homogeneous ice nucleation would still be the water activity criterion.[56]

3.2 Aqueous levoglucosan particles

The analysis of homogeneous ice nucleation from aqueous levoglucosan particles follows the same approach as the analysis of the aqueous $(NH_4)_2SO_4$ particles. Monodisperse and polydisperse particle distributions were applied in these experiments. The filled circles in Fig. 8 indicate the initial mean preparation conditions with respect to temperature, T_{prep}, and RH. The homogeneous ice nucleation experiments were conducted in the same manner as the freezing experiments of aqueous $(NH_4)_3SO_4$ particles. The freezing and melting temperatures and diameters for over 800 individual particles were digitally recorded and analyzed.

Fig. 8a presents the mean melting temperatures, $\bar{T}_{melt}$, including 1 standard deviation in uncertainty (open squares) and calculated median freezing temperatures with corresponding 20th and 80th percentiles, T_{freeze}, (filled squares) as a function of a_w at the preparation temperature, *i.e.* it is assumed that a_w does not change with temperature. The data presented in Fig. 8a indicate that for $a_w < 0.95$ the

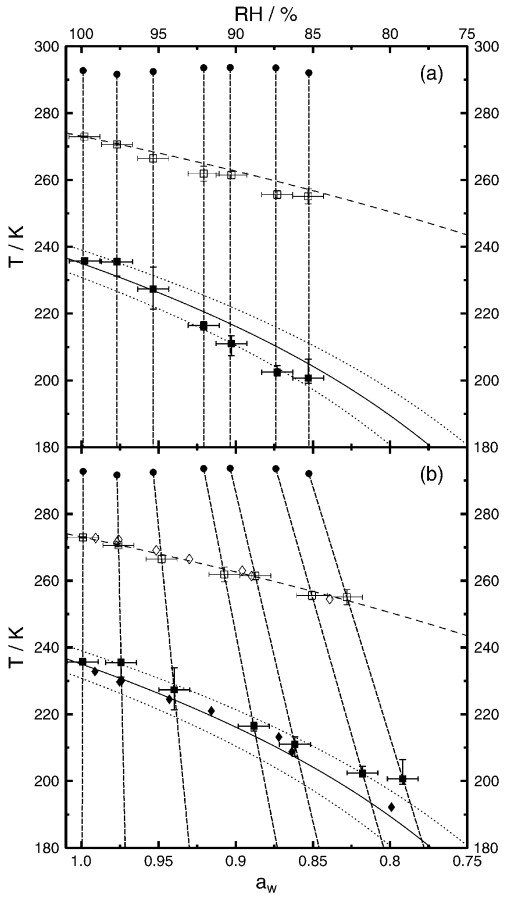

Fig. 8 Mean ice melting temperatures and median ice freezing temperatures with corresponding 20th and 80th percentiles are shown as open and solid squares, respectively, for aqueous levoglucosan particles prepared at 99.9, 97.7, 95.3, 92.1, 90.4, 87.4, and 85.3% RH. Solid circles indicate the mean preparation conditions with respect to temperature and RH. The wide dashed line and solid line represent the ice melting and homogeneous ice nucleation curve, respectively, given by Koop *et al.*[56] Dotted lines indicate the uncertainty in the homogeneous ice nucleation curve assuming $\delta(\Delta a_w) = \pm 0.025$. Panel (a): narrow dashed lines indicate constant a_w values. Panel (b): narrow dashed lines indicate changes in particle a_w with temperature employing eqn (10).[65] Open and solid diamonds represent ice melting and ice freezing data of aqueous levoglucosan particles,respectively, obtained from DSC measurements.[65]

corresponding $\bar{T}_{melt}$ values and T_{freeze} values are lower than the ice melting and freezing curves, respectively. Since homogeneous ice nucleation is a process of stochastic nature, it can be expected that T_{freeze} values lie within a broader temperature range.[9] However, the ice melting point is thermodynamically defined[88] and, hence, its accuracy is only constrained by the observation technique. A possible explanation for the systematic deviation of the measured $\bar{T}_{melt}$ values from the expected melting curve could be due to a strong temperature dependency of a_w for the aqueous levoglucosan solutions. Zobrist *et al.*[65] measured homogeneous ice freezing and corresponding ice melting temperatures of aqueous levoglucosan droplets located within an oil-matrix using DSC. These data are shown in Fig. 8b as diamonds. Zobrist *et al.*[65] derive a parametrization for a_w as a function of levoglucosan

concentration and temperature using their ice melting temperatures and previous water activity data:[89]

$$a_w(w_{lev}, T) = \frac{1 - 0.99918 w_{lev}}{1 - 0.90978 w_{lev} + 0.021448 w_{lev}^2} + (T - T^{\Theta})(-0.00045933 w_{lev} + 0.0035813 w_{lev}^2 + 0.00026549 w_{lev}^3 - 0.0033059 w_{lev}^4), \quad (10)$$

where w_{lev} is the mass weight fraction of levoglucosan in the aqueous solution and T^{Θ} = 298.15 K. This parametrization is employed here and extrapolated to yield a_w values for temperatures below the ice melting temperatures.[65] Since w_{lev} of the droplets employed in this study is not known, w_{lev} was derived by solving eqn (10) iteratively for known a_w values at the preparation temperature, T_{prep}. Aqueous particles prepared at 99.9, 97.7, 95.3, 92.1, 90.4, 87.4 and 85.3% RH correspond to 1.2, 19.9, 33, 45.8, 50.9, 58 and 62 wt% levoglucosan, respectively. Subsequently, eqn (10) was employed for the calculation of a_w for $T < T_{prep}$ for each of the aqueous levoglucosan particles.

Fig. 8b shows the experimentally derived ice melting and ice freezing temperatures for which changes in a_w according to eqn (10) were taken into account. The experimentally derived melting temperatures are in much better agreement with the ice melting curve. Also, the observed ice freezing temperatures are in closer agreement with the homogeneous ice nucleation temperature curve given by Koop *et al.*,[56] except for aqueous levoglucosan particles prepared at 85% RH. Multiple experiments employing different individual samples prepared at 85% RH resulted in higher median freezing temperatures than predicted for this highly concentrated aqueous levoglucosan solution. However, some of these particles froze at temperatures as low as 184 K. Reasons for this result could be due to the polydisperse size distribution of the employed particles and high viscosity of the highly concentrated aqueous levoglucosan droplets[90] which may slow the ice crystallization process. The overall better agreement between experimentally derived and predicted ice freezing temperatures suggests a non-linear change in particle a_w with decreasing temperature for aqueous levoglucosan particles. For aqueous levoglucosan particles a_w decreases with decreasing temperature, in contrast to aqueous $(NH_4)_2SO_4$ particles for which a_w appears to increase with decreasing temperature as indicated in Fig. 5. The obtained ice freezing temperatures are in good agreement with the data by Zobrist *et al.*[65] except for the aqueous levoglucosan particles prepared at 85% RH as discussed above. The data indirectly support KO00 when taking the uncertainty of the homogeneous freezing temperature of $\delta(\Delta a_w) = \pm 0.05$ into account.

Fig. 9 shows experimentally derived J_{hom}^{up} values as a function of temperature for aqueous levoglucosan particles depicted in Fig. 8. The J_{hom}^{up} values were derived applying eqn (4). In Fig. 9a the experimentally derived J_{hom}^{up} values are compared to theoretically derived J_{hom} values applying eqn (5) and the water activity criterion

$$\Delta a_w(T) = a_w(T_{prep}) - a_w^{ice}(T), \quad (11)$$

i.e. particle a_w is fixed at T_{prep}.

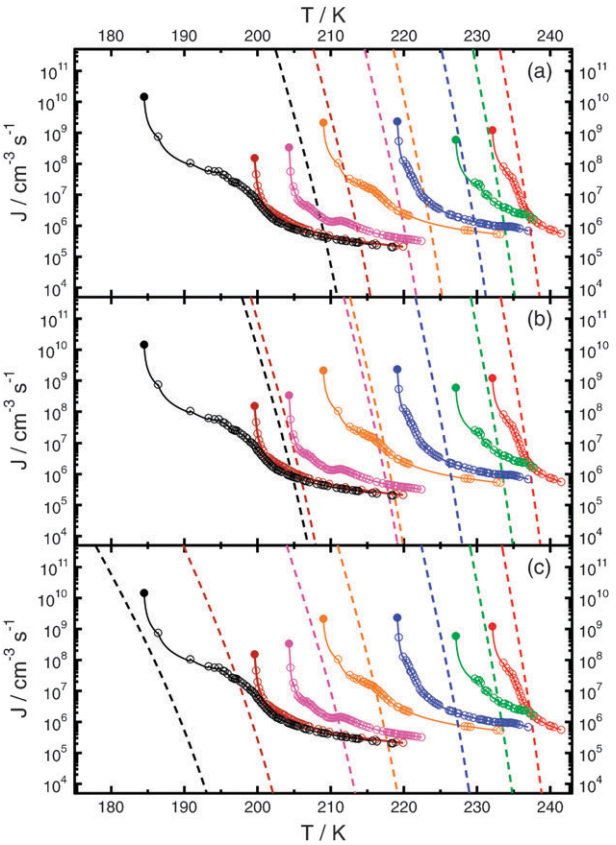

Fig. 9 Circles and dashed lines represent experimentally derived upper limits of the homogeneous ice nucleation rate coefficients and theoretically derived homogeneous ice nucleation rate coefficients,[56] respectively. The solid lines represent corresponding J_{hom}^{up} values obtained from integration of eqn (4). The colors red, green, blue, orange, magenta, brown and black correspond to aqueous levoglucosan particles prepared at 99.9, 97.7, 95.3, 92.1, 90.4, 87.4 and 85.3% RH, respectively. Solid circles represent the lowest observed freezing points of the respective aqueous levoglucosan particles. Panel (a): theoretically derived J_{hom} values are calculated applying the water-activity-based ice nucleation theory, assuming $\Delta a_w(T) = a_w(T_{prep}) - a_w^{ice}(T)$.[56] See text for more details. Panel (b): theoretically derived J_{hom} values are calculated applying the water-activity-based ice nucleation theory assuming $\Delta a_w(T) = a_w^{ice}(T_{melt}) - a_w^{ice}(T)$. See text for more details. Panel (c): theoretically derived J_{hom} values are calculated applying the water-activity-based ice nucleation theory assuming $\Delta a_w(T) = a_w(w_{lev},T) - a_w^{ice}(T)$. See text for more details.

Fig. 9a shows that the theoretically derived J_{hom} values are not compatible with the J_{hom}^{up} values. Predicted J_{hom} values are significantly larger than the J_{hom}^{up} values when approaching the lowest freezing temperature. However, assuming an uncertainty of $\delta(\Delta a_w) = \pm 0.025$, J_{hom} values agree for particles prepared at RH > 95%. For particles with lower initial a_w J_{hom}^{up} values deviate significantly from the predicted values.

The predicted J_{hom} values shown in Fig. 9b are derived assuming that $a_w(T_{freeze}) = a_w^{ice}(T_{melt})$. At the ice melting point of the frozen aqueous levoglucosan solution, a_w is in equilibrium with a_w^{ice}.[56] Accordingly, the a_w^{ice} values corresponding to T_{melt} are chosen as $a_w(T_{freeze})$. This case follows the approach by Koop *et al.*[56] where a_w at the melting point of the

solution determines a_w at the freezing point. J_{hom} values were derived according to eqn (5) applying

$$\Delta a_w(T) = a_w^{ice}(T_{melt}) - a_w^{ice}(T). \quad (12)$$

Fig. 9b clearly shows that the assumption of $\Delta a_w(T)$ given by eqn (12) does not yield satisfactory agreement. In particular for particles of lower a_w and thus higher levoglucosan concentrations, the deviations are still very large. However, for the most part the level of agreement is higher compared to the case depicted in Fig. 9a.

Fig. 9c shows the comparison of J_{hom} values for which the theoretically derived J_{hom} values were calculated applying the parameterization of $a_w(w_{lev},T)$ given by eqn (10).[65] J_{hom} values are calculated following the a_w trajectories given in Fig. 8b applying

$$\Delta a_w(T) = a_w(w_{lev},T) - a_w^{ice}(T). \quad (13)$$

Fig. 9c shows that this approach results in a closer agreement between theoretically derived J_{hom} values and experimentally derived J_{hom}^{up} values. Agreement is achieved for particles prepared with initial $a_w = 0.85$ and 0.87. For particles with $a_w > 0.87$ the predicted J_{hom} values come significantly closer to J_{hom}^{up} values but are still higher compared to the experimentally derived ones. These resulting small differences may be explained by the uncertainties in the prediction of a_w using an extrapolation from data obtained at much higher temperatures.

The results presented in Fig. 9 show that the J_{hom}^{up} values for homogeneous ice nucleation from aqueous levoglucosan particles can be represented by KO00 when significant changes in $a_w(T)$ are considered. The combination of determined ice freezing temperatures and J_{hom}^{up} values can be used as an accurate means to verify the water-activity-based ice nucleation theory.

4. Atmospheric implications

4.1 Ice particle production rates

It has been shown that biomass burning plumes can reach the UT/LS[42,43,48–50] where temperatures are low enough to induce homogeneous ice nucleation. Particle diameters of 90–2000 nm[42,50] and particle number densities of about 140 cm^{-3} were observed in biomass burning plumes.[42] Here it is assumed that the aqueous particles are composed mainly of levoglucosan. However, it cannot be ruled out that heterogeneous ice nucleation is another equally or even more important ice formation pathway within biomass burning plumes.[91,92] In contrast, the formation of a glass from aqueous levoglucosan particles may inhibit ice nucleation.[28,65]

For atmospheric applications such as interpretation of field data or modeling studies the ice particle number density produced from a pre-existing aerosol for given ambient temperatures and supersaturations with respect to ice, S_{ice}, is of concern. The experimentally derived J_{hom}^{up} values for aqueous levoglucosan particles can be applied to calculate maximum ice particle production rates, P_{ice}^{up} as a function of temperature, aqueous levoglucosan concentration, and ice supersaturation. $P_{ice}^{up}(T,w_{lev}) = V_{particle} J_{hom}^{up}(T,w_{lev})$, where $V_{particle}$ is the total particle volume per cm^3 of atmospheric air. $S_{ice}(w_{lev},T)$ is calculated according to

$$S_{ice}(w_{lev},T) = a_w(w_{lev},T)\frac{p^0_{H_2O}(T)}{p^{ice}_{H_2O}(T)}$$

where $p^{ice}_{H_2O}(T)$ is the water vapor pressure over ice at the given temperature.[73] It is assumed that eqn (10) is valid for temperatures below the ice melting points.[65] Assuming aqueous levoglucosan particles, 400 nm in diameter and in particle number densities of 140 cm^{-3},[42] with $a_w = 0.86$ and a freezing point of about 211 K, this would result in maximum ice particle production rates of 6.1×10^{-8} cm^{-3} s^{-1}. At this temperature S_{ice} is calculated as 1.51. The corresponding theoretical P_{ice} value derived applying KO00 is 5.6×10^{-6} cm^{-3} s^{-1}. The predicted P_{ice} values are in agreement with the experimentally derived values when an uncertainty of $\delta(\Delta a_w) = \pm 0.025$ is assumed, yielding an uncertainty of the predicted P_{ice} value of ± 6 orders of magnitude.

4.2 Water-activity-based ice nucleation theory

The water-activity-based ice nucleation theory can be used to predict homogeneous ice nucleation temperatures and corresponding ice nucleation rate coefficients for aqueous solution droplets without explicit knowledge of the solute.[56] This theory is based on experimental data which shows uncertainties in a_w as as high as $\delta(\Delta a_w) = \pm 0.05$.[57] The analysis given above shows that the homogeneous ice nucleation rate coefficients depend strongly on $a_w(c,T)$, with c being the solute concentration, which is experimentally inaccessible below T_{melt} but can be calculated using Pitzer ion-interaction models. However, these models fail for supercooled organic solutes. KO00 successfully captures the dependency of J_{hom} on a_w. However, Fig. 7 indicates that small changes in a_w by about 0.025 can shift the corresponding J_{hom} values by 6 orders of magnitude or 8 K in temperature. Since ice particle production rates are linearly related to J_{hom}, a similar range of uncertainties would result for corresponding P_{ice} values. More accurate predictions of a_w from supercooled aqueous solutions are necessary to decrease the corresponding uncertainty in J_{hom} when applying KO00. It should be kept in mind that different thermodynamic models result in different predictions of a_w. For example, Knopf *et al.* set up a Pitzer ion-interaction model which implemented newly obtained thermodynamic data for supercooled aqueous sulfuric acid solutions.[63] This model yielded a_w values for concentrated aqueous sulfuric acid solutions at temperatures of 180 K which are 10% lower in comparison to calculations by AIM.[61–63,86] This corresponds to a difference in Δa_w of 0.025. Such changes can result in differences of the J_{hom} values and corresponding P_{ice} values of up to 6 orders of magnitude.

5. Conclusions and summary

A new experimental method is introduced which allows us to study homogeneous ice nucleation from aqueous solution aerosol particles for which initial particle water activity instead of its composition is controlled. This approach mimics closer atmospheric conditions where particles composed of water soluble compounds adjust their composition according to the environmental relative humidity which then determines

particle water activity. Ice melting and homogeneous ice freezing temperatures of micrometre-sized aqueous $(NH_4)_2SO_4$ and aqueous levoglucosan particles and corresponding upper limits of the homogeneous ice nucleation rate coefficients were experimentally determined.

The experimentally derived freezing temperatures of aqueous $(NH_4)_2SO_4$ particles 5 to 39 wt% in concentration are in good agreement with the prediction of the water-activity-based ice nucleation theory.[56] Upper limits of the homogeneous ice nucleation rate coefficients of about 1×10^9 were determined for aqueous $(NH_4)_2SO_4$ particles. These experimentally derived homogeneous ice nucleation rate coefficients were compared to corresponding predictions of the water-activity-based ice nucleation theory[56] applying different approaches to estimate water activity for supercooled particles. The analysis presented here indicates a strong sensitivity of the predicted homogeneous ice nucleation rate coefficients on water activity. Differences between theoretically and experimentally derived homogeneous ice nucleation rate coefficients for aqueous $(NH_4)_2SO_4$ particles can be largely explained by accounting for expected uncertainties in particle water activity. More accurate water activity data of supercooled aqueous $(NH_4)_2SO_4$ solutions are needed to better constrain the predictions of the water-activity-based ice nucleation theory.

The experimentally derived ice melting and homogeneous ice freezing temperatures of aqueous levoglucosan particles with initial water activities of 0.85–0.99 are in good agreement with predictions by the water-activity-based ice nucleation theory when strong changes in particle water activity with temperature are taken into account.[65] These experiments yield upper limits of the homogeneous ice nucleation rate coefficients of about 1×10^8 to 1×10^{10} cm^{-3} s^{-1}. Predicted homogeneous ice nucleation rate coefficients come closer in agreement with experimentally derived upper limits of the homogeneous ice nucleation rate coefficients when a strong temperature dependence of particle water activity is employed and extrapolated to freezing temperatures. Remaining deviations between experimental data and predictions are most likely due to uncertainties in corresponding water activities. From the experimentally derived upper limits of the homogeneous ice nucleation rate coefficients maximum ice particle production rates as a function of ice supersaturation are estimated. For aqueous levoglucosan particles, 400 nm in diameter and particle number densities of 140 cm^{-3},[42,73] estimated maximum ice particle production rates are in agreement with predictions of the water-activity-based icenucleation theory if uncertainties in particle a_w are taken into account. The experimentally derived homogeneous ice nucleation rate coefficients can be applied to better constrain predictions of the water-activity-based ice nucleation theory.

This study clearly indicates the need to investigate homogeneous ice nucleation as a function of temperature and relative humidity employing the experimental methods discussed in Fig. 4 and others such as microdroplets levitated in electrodynamic balances[93–95] and aerosol cryo-chamber studies.[96,97] The newly presented experimental setup allows us to evaluate homogeneous ice nucleation from aqueous solutions as a function of water activity instead of particle composition. This experimental approach is particularly advantageous when studying complex aqueous inorganic/organic solution mixtures for which phase diagrams are not readily available and melting point measurements do not yield particle composition or the corresponding particle water activity.

Acknowledgements

D. Knopf acknowledges technical support by P. Varanasi. The authors appreciate helpful discussions with T. Koop and B. Zobrist. M. L. is grateful for financial support by the NSF CSEMS Grant DUE0422394. This work was supported by the NOAA Climate Program Office, Atmospheric Composition & Climate Program, Grant NA08OAR4310545.

References

1 P. Forster, V. Ramaswamy, P. Artaxo, T. Berntsen, R. Betts, D. W. Fahey, J. Haywood, J. Lean, D. C. Lowe, G. Myhre, J. Nganga, R. Prinn, G. Raga, M. Schulz and R. Van Dorland, in *Climate Change 2007: The Physical Science Basis. Contribution of Working Group I to the Fourth Assessment Report of the Intergovernmental Panel on Climate Change*, ed. S. Solomon, D. Qin, M. Manning, Z. Chen, M. Marquis, K. B. Averyt, M. Tignor and H. L. Miller, Cambridge University Press, 2007, ch. 2, p. 131.
2 S. Twomey, *Atmos. Environ.*, 1974, **8**, 1251.
3 S. Twomey, *Atmos. Environ. A*, 1991, **25**, 2435.
4 B. Albrecht, *Science*, 1989, **245**, 1227.
5 R. Pincus and M. Baker, *Nature*, 1994, **372**, 250.
6 M. B. Baker, *Science*, 1997, **276**, 1072.
7 D. Rosenfeld, *Science*, 2000, **287**, 1793.
8 V. Ramanathan, P. J. Crutzen, J. T. Kiehl and D. Rosenfeld, *Science*, 2001, **294**, 2119.
9 H. R. Pruppacher and J. D. Klett, *Microphysics of Clouds and Precipitation*, Kluwer Academic Publishers, Netherlands, 1997.
10 M. B. Baker and T. Peter, *Nature*, 2008, **451**, 299.
11 A. W. Brewer, *Q. J. R. Meteorol. Soc.*, 1949, **75**, 351.
12 J. R. Holton, P. H. Haynes, M. E. Mcintyre, A. R. Douglass, R. B. Rood and L. Pfister, *Rev. Geophys.*, 1995, **33**, 403.
13 U. Lohmann and E. Roeckner, *J. Geophys. Res.*, 1995, **100**, 16305.
14 I. M. Held and B. J. Soden, *Annu. Rev. Energ. Environ.*, 2000, **25**, 441.
15 E. Jensen and L. Pfister, *J. Geophys. Res.*, 2004, **109**, D02207.
16 T. Corti, B. P. Luo, Q. Fu, H. Vömel and T. Peter, *Atmos. Chem. Phys.*, 2006, **6**, 2539.
17 S. Fueglistaler and M. B. Baker, *Atmos. Chem. Phys.*, 2006, **6**, 1425.
18 J. Lelieveld, C. Brühl, P. Jockel, B. Steil, P. J. Crutzen, H. Fischer, M. A. Giorgetta, P. Hoor, M. G. Lawrence, R. Sausen and H. Tost, *Atmos. Chem. Phys.*, 2007, **7**, 1313.
19 S. Borrmann, S. Solomon, J. E. Dye and B. P. Luo, *Geophys. Res. Lett.*, 1996, **23**, 2133.
20 M. Krämer, C. Schiller, C. Voigt, H. Schlager and P. J. Popp, *Q. J. R. Meteorol. Soc.*, 2008, **134**, 905.
21 G. Vali, *J. Aerosol Sci.*, 1985, **16**, 575.
22 K. Sassen and G. C. Dodd, *J. Atmos. Sci.*, 1988, **45**, 1357–1369.
23 A. J. Heymsfield and R. M. Sabin, *J. Atmos. Sci.*, 1989, **46**, 2252.
24 J. Ström, M. Seifert, B. Kärcher, J. Ovarlez, A. Minikin, J. F. Gayet, R. Krejci, A. Petzold, F. Auriol, W. Haag, R. Busen, U. Schumann and H. C. Hansson, *Atmos. Chem. Phys.*, 2003, **3**, 1807.
25 W. Haag, B. Kärcher, J. Strom, A. Minikin, U. Lohmann, J. Ovarlez and A. Stohl, *Atmos. Chem. Phys.*, 2003, **3**, 1791.
26 P. J. DeMott, D. J. Cziczo, A. J. Prenni, D. M. Murphy, S. M. Kreidenweis, D. S. Thomson, R. Borys and D. C. Rogers, *Proc. Natl. Acad. Sci. U. S. A.*, 2003, **100**, 14655.
27 D. J. Cziczo, P. J. DeMott, S. D. Brooks, A. J. Prenni, D. S. Thomson, D. Baumgardner, J. C. Wilson,

S. M. Kreidenweis and D. M. Murphy, *Geophys. Res. Lett.*, 2004, **31**, L12116.
28 T. Peter, C. Marcolli, P. Spichtinger, T. Corti, M. B. Baker and T. Koop, *Science*, 2006, **314**, 1399.
29 R. W. Talbot, J. E. Dibb and M. B. Loomis, *Geophys. Res. Lett.*, 1998, **25**, 1367.
30 P. J. Adams, J. H. Seinfeld and D. M. Koch, *J. Geophys. Res.*, 1999, **104**, 13791.
31 B. R. T. Simoneit, *Appl. Geochem.*, 2002, **17**, 129–162.
32 Y. Iinuma, E. Brüggemann, T. Gnauk, K. Müller, M. O. Andreae, G. Helas, R. Parmar and H. Herrmann, *J. Geophys. Res.*, 2007, **112**, D08209.
33 W. Seiler and P. J. Crutzen, *Clim. Change*, 1980, **2**, 207.
34 J. A. Logan, M. J. Prather, S. C. Wofsy and M. B. Mcelroy, *J. Atmos. Chem.*, 1981, **86**, 7210.
35 P. J. Crutzen and M. O. Andreae, *Science*, 1990, **250**, 1669.
36 J. Fishman, K. Fakhruzzaman, B. Cros and D. Nganga, *Science*, 1991, **252**, 1693.
37 J. E. Penner, H. Eddleman and T. Novakov, *Atmos. Environ., Part A*, 1993, **27**, 1277.
38 C. Liousse, J. E. Penner, C. Chuang, J. J. Walton, H. Eddleman and H. Cachier, *J. Geophys. Res.*, 1996, **101**, 19411.
39 M. Scholes and M. O. Andreae, *Ambio*, 2000, **29**, 23.
40 G. Wotawa and M. Trainer, *Science*, 2000, **288**, 324.
41 A. E. Waibel, T. Peter, K. S. Carslaw, H. Oelhaf, G. Wetzel, P. J. Crutzen, U. Pöschl, A. Tsias, E. Reimer and H. Fischer, *Science*, 1999, **283**, 2064.
42 H. J. Jost, K. Drdla, A. Stohl, L. Pfister, M. Loewenstein, J. P. Lopez, P. K. Hudson, D. M. Murphy, D. J. Cziczo, M. Fromm, T. P. Bui, J. Dean-Day, C. Gerbig, M. J. Mahoney, E. C. Richard, N. Spichtinger, J. V. Pittman, E. M. Weinstock, J. C. Wilson and I. Xueref, *Geophys. Res. Lett.*, 2004, **31**, L11101.
43 M. Fromm, J. Alfred, K. Hoppel, J. Hornstein, R. Bevilacqua, E. Shettle, R. Servranckx, Z. Q. Li and B. Stocks, *Geophys. Res. Lett.*, 2000, **27**, 1407.
44 T. J. Duck, B. J. Firanski, D. B. Millet, A. H. Goldstein, J. Allan, R. Holzinger, D. R. Worsnop, A. B. White, A. Stohl, C. S. Dickinson and A. van Donkelaar, *J. Geophys. Res.*, 2007, **112**, D10S44.
45 S. Szidat, T. M. Jenk, H. A. Synal, M. Kalberer, L. Wacker, I. Hajdas, A. Kasper-Giebl and U. Baltensperger, *J. Geophys. Res.*, 2006, **111**, D07206.
46 Y. T. Hu, M. T. Odman, M. E. Chang, W. Jackson, S. Lee, E. S. Edgerton, K. Baumann and A. G. Russellt, *Environ. Sci. Technol.*, 2008, **42**, 3676.
47 J. K. Bein, Y. Zhao, M. V. Johnston and A. S. Wexler, *J. Geophys. Res.*, 2008, **113**, D07304.
48 P. K. Hudson, D. M. Murphy, D. J. Cziczo, D. S. Thomson, J. A. de Gouw, C. Warneke, J. Holloway, J. R. Jost and G. Hubler, *J. Geophys. Res.*, 2004, **109**, D23S27.
49 M. Fromm, R. Bevilacqua, R. Servranckx, J. Rosen, J. P. Thayer, J. Herman and D. Larko, *J. Geophys. Res.*, 2005, **110**, D08205.
50 D. M. Murphy, D. J. Cziczo, P. K. Hudson and D. S. Thomson, *J. Geophys. Res.*, 2007, **112**, D04203.
51 M. Posfai, A. Gelencser, R. Simonics, K. Arato, J. Li, P. V. Hobbs and P. R. Buseck, *J. Geophys. Res.*, 2004, **109**, D06213.
52 L. R. Mazzoleni, B. Zielinska and H. Mossmüller, *Environ. Sci. Technol.*, 2007, **41**, 2115.
53 O. L. Mayol-Bracero, P. Guyon, B. Graham, G. Roberts, M. O. Andreae, S. Decesari, M. C. Facchini, S. Fuzzi and P. Artaxo, *J. Geophys. Res.*, 2002, **107**, 8091.
54 W. F. Rogge, L. M. Hildemann, M. A. Mazurek, G. R. Cass and B. R. T. Simoneit, *Environ. Sci. Technol.*, 1998, **32**, 13.
55 J. J. Schauer, M. J. Kleeman, G. R. Cass and B. R. T. Simoneit, *Environ. Sci. Technol.*, 2001, **35**, 1716.
56 T. Koop, B. P. Luo, A. Tsias and T. Peter, *Nature*, 2000, **406**, 611.
57 T. Koop, *Z. Phys. Chem.*, 2004, **218**, 1231.
58 K. S. Pitzer, *Activity Coefficients in Electrolyte Solutions*, CRC Press, Boca Raton, FL, 2nd edn, 1991.
59 K. S. Carslaw, S. L. Clegg and P. Brimblecombe, *J. Phys. Chem.*, 1995, **99**, 11557.
60 M. Massucci, S. L. Clegg and P. Brimblecombe, *J. Phys. Chem. A*, 1999, **103**, 4209.
61 S. L. Clegg and P. Brimblecombe, *J. Phys. Chem. A*, 2005, **109**, 2703.
62 S. L. Clegg, P. Brimblecombe and A. S. Wexler, *J. Phys. Chem. A*, 1998, **102**, 2137.
63 D. A. Knopf, B. P. Luo, U. K. Krieger and T. Koop, *J. Phys. Chem. A*, 2003, **107**, 4322.
64 B. Zobrist, U. Weers and T. Koop, *J. Chem. Phys.*, 2003, **118**, 10254.
65 B. Zobrist, C. Marcolli, D. A. Pedernera and T. Koop, *Atmos. Chem. Phys.*, 2008, **8**, 5221.
66 T. Koop, H. P. Ng, L. T. Molina and M. J. Molina, *J. Phys. Chem. A*, 1998, **102**, 8924.
67 D. A. Knopf, T. Koop, B. P. Luo, U. G. Weers and T. Peter, *Atmos. Chem. Phys.*, 2002, **2**, 207.
68 M. Dymarska, B. J. Murray, L. M. Sun, M. L. Eastwood, D. A. Knopf and A. K. Bertram, *J. Geophys. Res.*, 2006, **111**, D04204.
69 D. A. Knopf and T. Koop, *J. Geophys. Res.*, 2006, **111**, D12201.
70 D. A. Knopf, *J. Phys. Chem. A*, 2006, **110**, 5745–5750.
71 A. K. Bertram, T. Koop, L. T. Molina and M. M. J., *J. Phys. Chem. A*, 2000, **104**, 584.
72 D. A. Knopf, PhD Thesis, Number 15103, Swiss Federal Institute of Technology Zurich, ETH Zentrum, Ramistrasse 101, 8092, Zurich, 2003.
73 D. M. Murphy and T. Koop, *Q. J. R. Meteorol. Soc.*, 2005, **131**, 1539.
74 *CRC Handbook of Chemistry and Physics*, ed. D. R. Lide, CRC Press, New York, 88th edn, 2007, pp. 1–524.
75 D. A. Knopf, P. Zink, J. Schreiner and K. Mauersberger, *Aerosol Sci. Technol.*, 2001, **35**, 924.
76 T. Koop, B. P. Luo, U. M. Biermann, P. J. Crutzen and T. Peter, *J. Phys. Chem. A*, 1997, **101**, 1117.
77 B. H. Larson and B. D. Swanson, *J. Phys. Chem. A*, 2006, **110**, 1907.
78 J. H. Chelf and S. T. Martin, *J. Geophys. Res.*, 2001, **106**, 1215.
79 D. J. Cziczo and J. P. D. Abbatt, *J. Geophys. Res.*, 1999, **104**, 13781.
80 A. J. Prenni, P. J. DeMott, S. M. Kreidenweis, D. E. Sherman, L. M. Russell and Y. Ming, *J. Phys. Chem. A*, 2001, **105**, 11240.
81 H.-M. Hung, A. Malinowski and S. T. Martin, *J. Phys. Chem. A*, 2002, **106**, 293.
82 Y. Chen, P. J. DeMott, S. M. Kreidenweis, D. C. Rogers and D. E. Sherman, *J. Atmos. Sci.*, 2000, **57**, 3752.
83 B. J. Murray, D. A. Knopf and A. K. Bertram, *Nature*, 2005, **434**, 202.
84 A. J. Prenni, M. E. Wise, S. D. Brooks and M. A. Tolbert, *J. Geophys. Res.*, 2001, **106**, 3037.
85 J. P. D. Abbatt, S. Benz, D. J. Cziczo, Z. Kanji, U. Lohmann and O. Möhler, *Science*, 2006, **313**, 1770.
86 D. A. Knopf, B. P. Luo, U. K. Krieger and T. Koop, *J. Phys. Chem. A*, 2005, **109**, 2707.
87 M. Baker and M. Baker, *Geophys. Res. Lett.*, 2004, **31**, L19102.
88 P. W. Atkins, *Physical Chemistry*, Freeman and Company, New York, 5th edn, 1994.
89 M. N. Chan, M. Y. Choi, N. L. Ng and C. K. Chan, *Environ. Sci. Technol.*, 2005, **39**, 1555.
90 B. J. Murray, *Atmos. Chem. Phys.*, 2008, **8**, 5423.
91 P. V. Hobbs and L. F. Radke, *Science*, 1969, **163**, 279.
92 K. Sassen and V. I. Khvorostyanov, *Environ. Res. Lett.*, 2008, **3**, 025006.
93 U. K. Krieger, C. A. Colberg, U. Weers, T. Koop and T. Peter, *Geophys. Res. Lett.*, 2000, **27**, 2097.
94 D. Duft and T. Leisner, *Atmos. Chem. Phys.*, 2004, **4**, 1997.
95 P. Stöckel, I. M. Weidinger, H. Baumgärtel and T. Leisner, *J. Phys. Chem. A*, 2005, **109**, 2540.
96 P. Zink, D. A. Knopf, J. Schreiner, K. Mauersberger, O. Möhler, H. Saathoff, M. Seifert, R. Tiede and U. Schurath, *Geophys. Res. Lett.*, 2002, **29**, 1551.
97 O. Möhler, S. Stetzer, S. Schaefers, C. Linke, M. Schnaiter, R. Tiede, H. Saathoff, M. Krämer, A. Mangold, P. Budz, P. Zink, J. Schreiner, K. Mauersberger, W. Haag, B. Kärcher and U. Schurath, *Atmos. Chem. Phys.*, 2003, **3**, 211.
98 L. Greenspan, *J. Res. Natl. Bur. Stand., Sect. A*, 1977, **81**, 89.
99 I. N. Tang and H. R. Munkelwitz, *Atmos. Environ., Part A*, 1993, **27**, 467.
100 J. Xu, D. Imre, R. McGraw and I. Tang, *J. Phys. Chem. B*, 1998, **102**, 7462.
101 T. B. Onasch, R. L. Siefert, S. D. Brooks, A. J. Prenni, B. Murray, M. A. Wilson and M. A. Tolbert, *J. Geophys. Res.*, 1999, **104**, 21317.

